Heat Mass Transfer (2006) 43: 135–148
DOI 10.1007/s00231-006-0100-3

ORIGINAL

S. A. Nada

Slot/slots air jet impinging cooling of a cylinder for different jets–cylinder configurations

Received: 10 June 2005 / Accepted: 25 January 2006 / Published online: 14 February 2006

Abstract Heat transfer characteristics of a slot/slots jet air impinging on a cylinder have been experimentally investigated for two different orientations of slot/slots jet plan with respect to cylinder axis. The experiments were carried out to study the effects of orientation of slot/slots jet plan with respect to cylinder axis on the rate of heat transfer from the cylinder. Two different jet–cylinder configurations were studied: (1) single slot jet aligned with cylinder axis (slot length = cylinder length), and (2) multiple slot jets equally spaces distributed orthogonal to cylinder axis (each slot length = cylinder diameter and sum of slots lengths = cylinder length). For each configuration, parametric effects of Reynolds numbers (Re) ranging from 1,000 to 10,000, dimensionless slot widths (W/d) ranging from 0.125 to 0.5, and dimensionless slot orifice-to-cylinder spacing (Z/W) ranging from 1 to 12 on local and average Nusselt numbers around cylinder surface have been investigated. The results showed that: (1) cooling the cylinder by multiple slots jets situated orthogonal to cylinder axis gave more uniform surface temperature distributions and higher heat transfer rate than the case of cooling the cylinder by single slot jet aligned with cylinder axis, (2) for both configurations the Nusselt number around the cylinder increased with increasing Re and W/d, and (3) for both configurations there was a certain Z/W in the range $4 < Z/W < 6$ at which the stagnation and mean Nusselt number were maximum. Correlations for the mean Nusselt numbers around cylinder surface have been presented for both configurations. Comparisons between the correlations predictions and the present and other previous experimental data have been conducted.

S. A. Nada
Mechanical Engineering Department,
Benha High Institute of Technology,
Benha 13512, Egypt
E-mail: samehnadar@yahoo.com
Tel.: +20-12-1723182
Fax: +20-13-3230297

List of symbols

A	Cylinder surface area
A_s	Slot area
d	Cylinder diameter
H	Height of potential core
h	Local heat transfer coefficient
$\bar{h}_c$	Circumferential average heat transfer coefficient
I	Electric current
k_a	Thermal conductivity of air
L	Cylinder length
$\dot{m}$	Air mass flow rate
n	Number of slots
Nu	Local Nusselt number
$\overline{Nu}$	Average Nusselt number
$\overline{Nu}_c$	Circumferential average Nusselt number
$\Delta\overline{Nu}$	Uncertainty in Nusselt number
q	Rate of heat transfer from the cylinder by convection
q_r	Rate of heat losses by radiation
Re	Reynolds number based on cylinder diameter
T	Local temperature at cylinder surface
$\bar{T}$	Average surface temperature of the cylinder
T_a	Air temperature at the slot exit
T_∞	Ambient temperature (°C)
V	Voltage
v	Average jet exit velocity
W	Slot width
x	Axial distance along the cylinder
Z	Slot orifice-to-cylinder spacing
θ	Circumference angle measured from impinging point
ε	Emissivity
σ	Stefan–Boltzmann constant
υ	Kinematics viscosity

1 Introduction

Jet impingement cooling technique is encountered in many engineering applications and manufacturing

processes such as cooling of gas turbines blades, annealing of metals and glass, textiles and paper drying, heating, cooling or drying of painted cylinders and foodstuffs, de-icing of aircraft wings and cooling of high power density electronic equipments. Jet impingement cooling has the advantages of its low cost, simple control, and its high local heat transfer rate at the impinging point.

Over the past 40 years, large numbers of publications on jet impinging cooling of a flat surface were conducted. These studies were carried out for different types of jets, namely: free, confined or semi-confined jets having different orifices exit geometries. A number of critical reviews and bibliographical works on various aspects of experimental, analytical, and numerical works of flow and heat transfer characteristics of jet impingement cooling of a flat surface have been published [1–6]. These literature reviews had highlighted that studies related to impingement cooling over curved surfaces are relatively few.

Heat transfer characteristics of jet impingement cooling of curved gas turbine airfoil blades have been studied by many investigators [7–10] to show the effects of jets geometries, blade geometries, jet–blades configurations, and air Reynolds number on the rate of heat transfer. Also, impingement cooling of a semi circled concave surface has studied by many other investigators [11–13]. In these studies the effects of jet-to-jet spacing, distance between the jet and the cooled surface, and various jet-hole arrangements were studied. Dyban and Mazur [14] measured heat transfer coefficient on a parabolic concave surface and studied the effects of jet flow passage curvature. Kayansyan and Kucuka [15] carried out an experimental and numerical study for jet impingement cooling of a concave channel when the slot jet was situated at the symmetry line of a semicircular channel. A correlation for the stagnation region heat transfer coefficient was presented to account for the channel height effect. Also, Yang et al. [16] studied jet impingement cooling on concave surface for three different nozzle configurations. The effects of nozzle shapes, surface curvature, Reynolds numbers, and spacing between the nozzle exit and the cooled surface were of primary interests. Markedly different flow and heat transfer characteristics have been observed when different nozzles were used. The effect of curvature noticed to be more prominent as Reynolds number increases. Choi et al. [17] have studied fluid flow and heat transfer characteristics of a slot jet impingement on a semi-circular concave surface. They have laid the emphasis on interpreting the heat transfer data in association with the measured mean velocity and velocity fluctuations of impinging and evolving wall jet region along the concave surface. Gau and Chung [18] performed experiments on two dimensionally free jet impinging normally on a concave and on a convex semi-cylindrical heated surfaces to study the surface curvature effect on the different sizes of slot air jet impingement cooling flow structure and heat transfer around these surfaces. In the concave surface case, they concluded that the increase in the curvature increases the convective heat transfer rate. In the convex surface case, it was found that a series of three-dimensional counterrotating vortices around the surface could increase the momentum transport in the flow structure and enhance the heat transfer process on the wall near the stagnation point. The increase of the surface curvature could augment the size of the counterrotating vortices, which produced a higher Nusselt number at stagnation point. However, the heat transfer magnitude was reduced in the region away from the stagnation point where the flow becomes more stable due to the centrifugal force around the surface curvature. Recently, Lee et al. [19] have investigated the effects of the hemispherical convex surface curvature on the heat transfer and flow from a fully developed axisymmetric impinging jet. They noticed that the Nusselt number at the stagnation point increased with increasing the surface curvature. However, the effect of surface curvature on the heat transfer was found less on the wall jet region compared to its stagnation point region. Chan et al. [20] investigated surface heat transfer characteristics of a heated slot jet impinging on a semi-circular convex surface by using the transient heating liquid crystal technique. The effects of jet Reynolds number and the slot nozzle-to-impingement surface distance on the local circumferential heat transfer have been studied. Correlations of local and average Nusselt numbers were presented for the stagnation point and the circumferential distribution.

Only limited papers concerning jet impingement heat transfer on the outside surface of a complete cylinder have been identified. In these studies the jet plane was aligned with the axis of the cylinder. Potts [21] has studied flow filed and heat transfer characteristics of cooling cylinders by round turbulent jet impingement. The relationship between the radius of the nozzle and that of the cylinder was found to be a vital parameter on the process of cooling. Sparrow et al. [22] have investigated jet impingement heat transfer for a circular jet impinging in cross-flow on a cylinder. They reported that the axial distribution of the local heat transfer coefficient peaked at the jet impingement point. Gori and Bossi [23] have studied heat transfer of slot jets of air impinging on the surface of a circular cylinder when the jet plane was aligned with the axis of the cylinder. The cylinder had a diameter of $d = 10$ mm and the slot jet had a width of 5 mm. The effects of air Reynolds number and the distance between the exit of the slot jet and the cylinder on the local Nusselt number have been investigated. Correlations for mean Nusselt numbers were presented. Also, Sparrow and Alhomoud [24] have measured heat transfer coefficient for a circular cylinder subjected to impingement of a slot jet. In one set of their experiments, the symmetry plane of the jet was aligned with the axis of the cylinder, while in other experiments the jet was offset from the cylinder. In addition of the offset, parametric variation was also studied for the width of the jet, the distance between the slot and the

cylinder and the Reynolds number. McDaniel and Webb [25] have studied the heat transfer characteristics of circular cylinder exposed to air slot jet impingement whose plane aligned with the axis of the cylinder. Both contoured orifice and sharp-edged orifice jet configurations were investigated for different jet widths, Reynolds numbers and distances between the cylinder and the jet orifice. The average heat transfer coefficient of the cylinder was correlated for the different jet geometries. Recently, Olsson et al. [26] have studied heat transfer from a slot air jet impinging on a cylinder shaped food product placed on a solid surface in a semi-confined area using computational fluid dynamics (CFD). The slot jet plane was aligned with the axis of the cylinder. The distribution of the local Nusselt numbers around the cylinder for various Reynolds numbers, jet-to-cylinder distances, and cylinder curvatures were determined. The results showed that the local Nusselt numbers varies around the surface of the cylinder and that the average Nusselt number and the stagnation point Nusselt number increases with increasing Reynolds numbers and surface curvatures but has little dependency on the jet-to-cylinder distances. Correlations for Nusselt numbers were presented. Also, Olsson et al. [27] have presented computational study of flow and heat transfer predictions of multiple slot air jets impinging on circular cylinders placed on a horizontal surface using CFD. Each slot jet was situated so that its plane was aligned with the axis of a cylinder. The distribution of Nusselt numbers around the cylinders for different Reynolds numbers, distances between the cylinders and slot jet openings were determined for two and three jets and compared to the simulation of a single jet. Correlations for heat transfer coefficients were presented.

As shown above, all previous studies concerning jet impingement cooling of complete cylinders were carried out with the jet plane aligned with the axis of the cylinder. To the author's knowledge, no previous studies have covered the case of cooling cylinders by multiple slot jets impingement whose slots plane aligned orthogonal to the axis of the cylinder. Therefore, the aim of the present work is to study heat transfer from circular cylinder cooled by air slot jets impingement for two different jet–cylinder configurations as shown in Fig. 1. In the first configuration, a single long slot jet - aligned with cylinder axis cools the cylinder. The length of the slot jet equals the length of the cylinder. This configuration is termed in the paper as configuration 1. In the second configuration, the cylinder is cooled by multiple slot jets aligned orthogonal to the axis of the cylinder. The length of each slot equals to the diameter of the cylinder. This configuration is termed in the paper as configuration 2. For comparison study, the number for slot jets in configuration 2 was chosen to give sum of their lengths equals the length of the single slot jet of configuration 1, i.e., $n = L/d$. In configuration 2, the multiple jets were situated equally spaces along the axis of the cylinder. For each configuration, the effects of Reynolds numbers, slot jet widths, and jet-to-cylinder spaces on the distribution of the Nusselt numbers around the cylinder surface were investigated. Correlations of Nusselt numbers in terms of the relevant parameters were presented for the two configurations. Comparison between the two configurations was studied under the same conditions.

2 Experimental apparatus and procedure

2.1 Experimental setup

A schematic diagram of the experimental slot air jet cooling system of a cylinder is shown in Fig. 2. To ensure high air quality, air from a compressor was supplied to an air storage tank, then passed through air filtering system, air dryer, a high precision regulator, a hand-operated

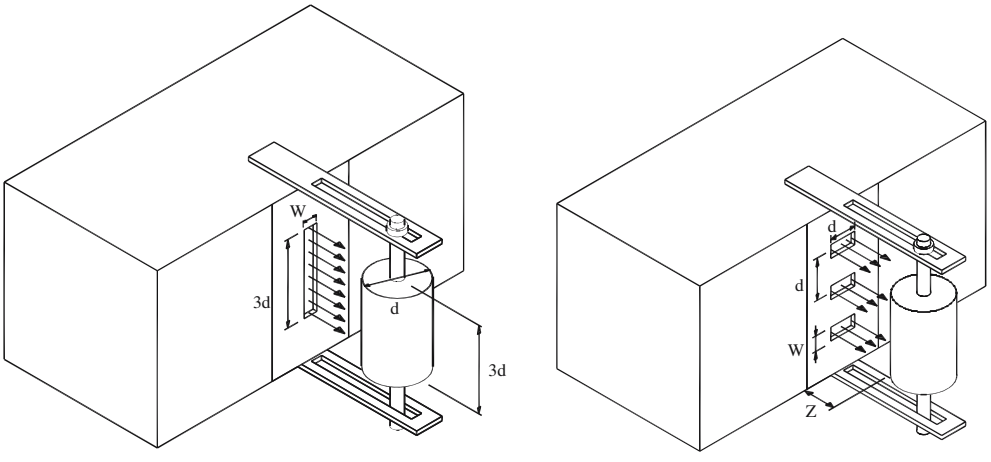

(a) Configuration1

(Single slot jet aligned with cylinder axis)

(b) Configuration 2

(Multiple slots jets orthogonal to cylinder axis)

Fig. 1 Different jets–cylinder configurations. **a** Configuration 1 (single slot jet aligned with cylinder axis). **b** Configuration 2 (multiple slots jets orthogonal to cylinder axis)

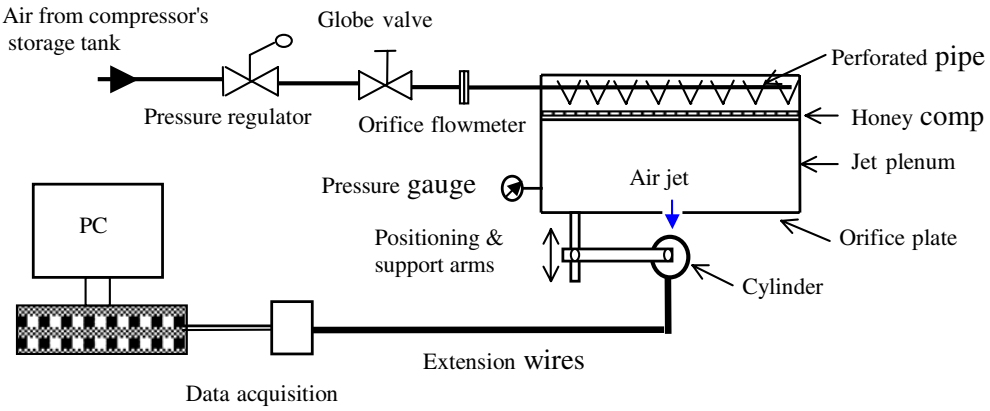

Fig. 2 Schematic diagram of slot air jet cooling system

global valve, an orifice flow meter, and finally entered a jet plenum. The required air pressure and flow rate were controlled by the pressure regulator and the hand-operated global valve. Two pressure gauges were used to measure air pressure at the orifice meter and in the jet plenum. The airflow rate was measured by the orifice flow meter with a digital manometer across the orifice. The orifice flow meter was calibrated using a laminar flow element with an accuracy of $\pm 2\%$. Air enters the jet plenum through a perforated air supply pipe, and then passes through a honeycomb and turbulence eliminating screens to straighten the flow and produce uniform velocity profile at the slot orifice exit. The jet plenum was a 10-mm thick Plexiglas airtight box with outside dimensions $600 \times 300 \times 300$ mm. The front face of the box contains an opening of dimensions 300×80 mm at the center. Different Plexiglas orifice plates containing slots of different widths and orientations were fitted and glued in this opening according to the experimental program. The slot orifice exit geometry was a sharp edge. Two sets of orifice plates were used. The first set contained three orifice plates, each had a longitudinal slot opening of length 150 mm (equal cylinder length), of slot widths 25, 12.5, and 6.25 mm, respectively. The slot was positioned at the center of each orifice plate as shown in Fig. 1a. The second set contains another three orifice plates; each had three traverse slots of lengths 50 mm (equal to the diameter of the cylinder), of slot widths 25, 12.5, and 6.25 mm, respectively. The three traverse slots of each orifice plate are positioned equally spaced along the orifice plate as shown in Fig. 1b. The airflow exiting from the honeycomb passes through the slot or slots opened in the orifice plate impinging the heated cylinder (test section) which was aligned parallel to the longitudinal axis of the orifice plate at a separated distance Z (see Fig. 1). The heated cylinder was suspended to the plenum box by positioning and support arms attached to the walls of the plenum box as shown in Fig. 2. The separation distance between the cylinder and the orifice plate (Z) was adjusted using the positioning arms. To obtain one of the two configurations of cooling the cylinder by single slot jet aligned along the axis of the cylinder or by multiple slot jets aligned normal to the axis of the cylinder, an orifice plate of the first set or of the second set was inserted in the opening side of the plenum box, respectively.

The test section (heated cylinder) consisted of a copper circular cylinder of 50-mm outside diameter and 2-mm thickness. The length of the cylinder was 150 mm. A ceramic circular rod of 25-mm diameter and 150-mm length was centrally inserted inside the cylinder. A flat electric resistance Nickel–Chrome heating wire was wrapped around the ceramic rod to generate the required input heat to the cylinder. The electric heater wire was insulated with mica insulating tape. The gap between the ceramic rod and the inner surface of the cylinder was filled with fine sand to be sure of uniform heating of the cylinder. The ends of the cylinder were caped by Teflon pugs to prevent heat losses from the ends of the cylinder. Figure 3 shows a cross-sectional view of the test section. The resistance heating wire was connected with a DC power supply to control the power input to the cylinder. The input voltage and current were controlled by the fine tunings of the power supply to keep the input power density constant at 0.192 W/cm^2 through all the experiments. The voltage and the current drawn were measured by digital voltmeter and digital ammeter with ± 0.01 V and ± 0.01 accuracy, respectively. The axial and circumferential temperature distributions on the outside surface of the cylinder were measured using 45 thermocouples (K-type) mounted at five axial locations of the cylinder. Each axial location contains nine thermocouples equal spaces distributed along half of the circumference of the cylinder as shown in Fig. 3. The thermocouples junctions were fitted in the tube thickness and fixed using fine tin solders. The thermocouples weirs were extended through the gap between the cylinder and the ceramic rod. Two other thermocouples were used to measure the exit air temperature at the orifice plate and the surrounding temperature. All the thermocouples were calibrated in a constant temperature path and a measurement accuracy of ± 0.1°C was obtained. All the temperature signals were acquired with a data acquisition system and sent into a PC for data recording.

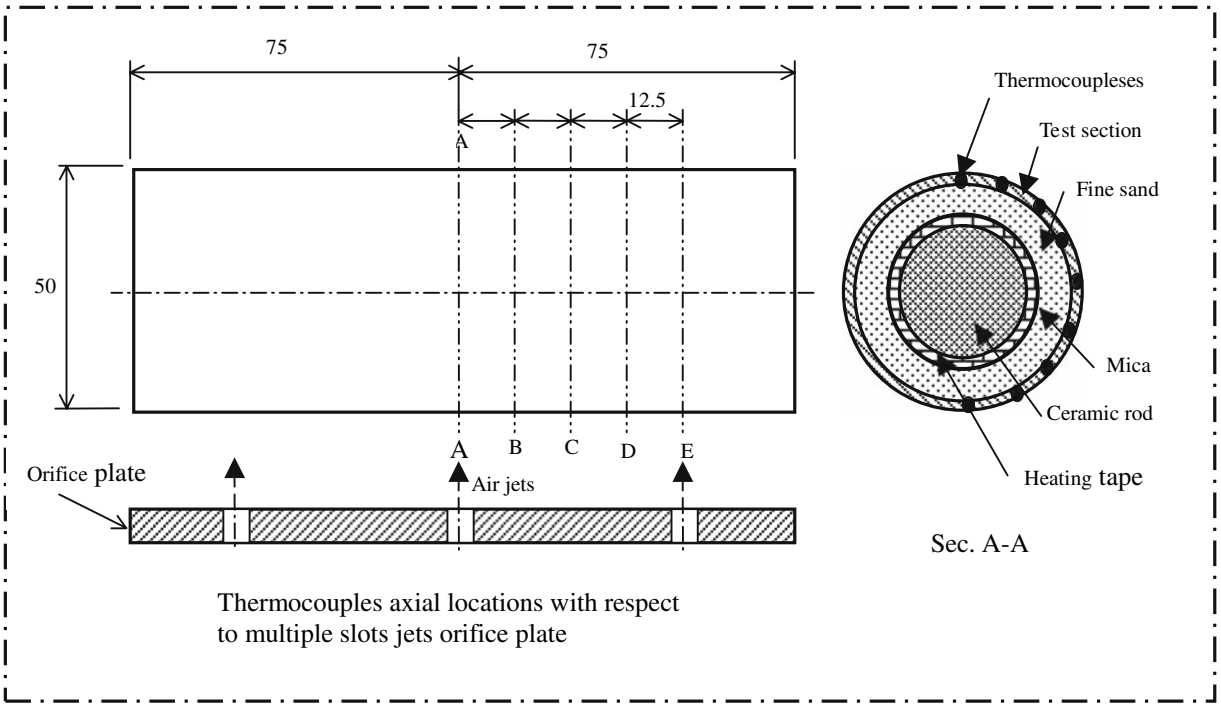

Fig. 3 Cross-section view and thermocouples distributions of heated cylinder

2.2 Experimental conditions

The ranges of the test variables used in this study were:

Cylinder diameter	50 mm
Heating power density	0.192 W/cm^2
Air Reynolds number (Re) based on cylinder diameter and average air velocity at slot exit	1,000–10,000
Dimensionless slot width (W/d)	0.125–0.5
Dimensionless separation distance between cylinder and jet orifice plate (Z/W)	1–12

2.3 Experimental procedure and program

The procedure and experimental program for each of the two studied jet–cylinder configurations were as follows:

1. Insert and glue the orifice plate that has the required slot width (W/d) in it's opening in the plenum.
2. Adjust the separation distance Z/W between the cylinder and the orifice plate to the required value.
3. Supply and adjust power to the cylinder.
4. Open airflow, adjust the required Reynolds number and allow air jet to impinge the cylinder surface.
5. Wait until steady state condition is achieved. The steady state condition was achieved when the differences in the measured temperatures were not more than 0.2 °C over 20 min.
6. Record all instruments readings (voltage, current, pressures, and temperatures).
7. Repeat steps 4–6 for different Reynolds numbers (1,000, 2,500, 4,000, 5,500, 7,000, 8,500, and 10,000).
8. Repeat steps 2–7 for different separation distances Z/W (1, 2, 4, 8, and 12).
9. Repeat steps 1–8 for different slot widths W/d (0.125, 0.25, and 0.5).

2.4 Data reduction

The Reynolds number (Re) based on the cylinder diameter was calculated from the measured airflow rate using the equations:

$$Re = \frac{vd}{\upsilon}, \tag{1}$$

where v is the average jet exit velocity ($v = \dot{m}/\rho A_s$), d is the cylinder diameter, υ and ρ is the kinematics viscosity and density of the air at the jet exit, $\dot{m}$ is the air mass flow rate and $A_s$is the area of the slot.

The energy balance for the heated cylinder gives

$$VI = q + q_r, \tag{2}$$

where I and V are the electric current and voltage input to the cylinder, q is the heat transfer by convection from the cylinder, and q_r is the heat transfer by radiation from the cylinder to the surroundings. The radiation heat transfer was calculated from the following equation assuming that the surrounding is a black body at the ambient temperature and completely surround the cylinder:

$$q_r = \pi dL\sigma\varepsilon((\bar{T} + 273)^4 - (T_\infty + 273)^4), \tag{3}$$

where $\bar{T}$, ε, L, σ, and T_∞ are cylinder average temperature, ε cylinder emissivity (polished copper), cylinder length, Stefan–Boltzmann constant and surrounding temperature, respectively. The radiation heat transfer from the cylinder was within 2% of the input heat during all the experiments.

The local convection heat transfer coefficient at a point on the cylinder surface is given by:

$$h = \frac{q}{\pi dL(T - T_a)}, \tag{4}$$

where T is the local temperature at this point and T_a is the air temperature at the jet exit. In calculating the circumferential average heat transfer coefficient at a certain axial location of the cylinder, half of the circumference of the cylinder (the second half is symmetrical to it) was divided into eight-equal sectors as shown in Fig. 3. The circumferential average heat transfer coefficient ($\bar{h}_c$) at a certain axial location x can be expressed as

$$\bar{h}_c = \frac{q}{8A}\sum_{i=1}^{8}\frac{1}{(T_i - T_a)}, \tag{5}$$

where T_i is the temperature of ith circumferential sector of the cylinder. It was taken as the average of the two-thermocouple readings on the boundary of this sector. The circumferential average Nusselt number ($\overline{Nu}_c$) at this axial location is defined as

$$\overline{Nu}_c = \frac{qd}{8A}\sum_{i=1}^{8}\frac{1}{k_{ai}(T_i - T_a)}, \tag{6}$$

where $k_a i$ is the thermal conductivity of the air taken at $(T_i + T_a)/2$.

The physics of the jet and the temperature measurements of the present work showed that there is no axial temperature variation for the configuration of using a single slot jet aligned along the axis of the cylinder. In this case the average Nusselt number along the cylinder ($\overline{Nu}$) is equal to the circumferential average Nusselt number ($\overline{Nu}_c$). However there was axial temperature variation along cylinder surface between each two successive jets in the case of using multiple slot jets aligned orthogonal to the axis of the cylinder. In this case, to calculate the average Nusselt number along the cylinder, the mean of the average circumferential Nusselt numbers at the five axial locations between the two successive jets where the thermocouples were fixed on the cylinder was taken as follows:

$$\overline{Nu} = \frac{1}{5}\sum_{j=1}^{5}\overline{Nu}_{cj} \tag{7}$$

Combining (2), (3), (4), (5), (6), and (7) together, the expression of $\overline{Nu}$ is as follows:

$$\overline{Nu} = \left[VI - \pi dL\sigma\varepsilon\left((\bar{T} + 273)^4 - (T_\infty + 273)^4\right)\right] \times \frac{1}{5\pi L}\sum_{j=1}^{5}\sum_{i=1}^{8}\frac{1}{k_{ai}(T_i - T_a)}. \tag{8}$$

The last equation is in the form

$$\overline{Nu} = f(x_1, x_2, x_3, \ldots, x_n), \tag{9}$$

where x_1 to x_n are the all variables that affect the experimental determination of $\overline{Nu}$. The uncertainty $\Delta\overline{Nu}$ in the value of $\overline{Nu}$ was estimated based on the procedure of Holman and Gajda [28] and is expressed as follows

$$(\Delta\overline{Nu})^2 = \sum_{i=1}^{n}\left(\frac{\partial\overline{Nu}}{\partial x_i}\Delta x_i\right)^2, \tag{10}$$

where Δx_i is the uncertainty in the x_i variable. The uncertainty in the various variables used in the determination of the Nusselt number were 0.25% for the electric current I, 0.25% for the electric volt V, 0.1°C for temperature differences, 0.001 m for any distance measurement, 0.5% for the thermal conductivity of air, and 5% for the emissivity of the cylinder. It was found that the uncertainty for the data of $\overline{Nu}$ ranges from 4 to 7% depending on the values of Re, W/d, and Z/W.

3 Results and discussions

3.1 Local distribution of Nusselt number

Figure 4 presents the circumferential variation of the local Nusselt number versus the angle θ (measured from the impinging point) with the Reynolds number as a parameter for configuration 1 at $Z/W = 4$ and $W/d = 0.25$. The angle θ varies in the range of $0° < \theta < 180°$ for half of the circumference of the cylinder. The other half ($-180° < \theta < 0°$) is symmetric to it. Figure 4 shows that, at any Reynolds number, the local Nusselt number had its maximum value at the impinging point ($\theta = 0°$) and then decreased with increasing θ in the range $0° < \theta < 135°$. This can be attributed to the higher jet velocity that causes high heat transfer in the stagnation zone. Then the heat transfer decreased over the curved surface with increasing θ due to the reduction of the flow velocity. Also Fig. 4 shows that the local Nusselt number was minimum and approximately constant in the range $135° < \theta < 180°$. This trend is consistent with the results of the experiments of Gori and Bossi [23] for a slot jet flow around a cylinder. In their work the minimum local Nusselt number was found at $\theta = 180°$ for $Re < 10{,}000$ and in the range $135° < \theta < 180°$ for Re around 13,000. A relative minimum of the circumferential variation of local Nusselt number was never noticed in the present work for any value of W/d and Z/W. Gori and Bossi [23], Gau and Chung [18] and Olsson et al. [26] reported a relative minimum of the local Nusselt number at $\theta = 90°$. This contradiction can be attributed to the low range of Re of the present study ($Re < 10{,}000$). An accurate examination of the data of Gori and Bossi [23] for $Re < 10{,}000$ reveals that a relative minimum did not exist for $Re < 10{,}000$, which supports our results. Also Fig. 4 shows that the variation in the

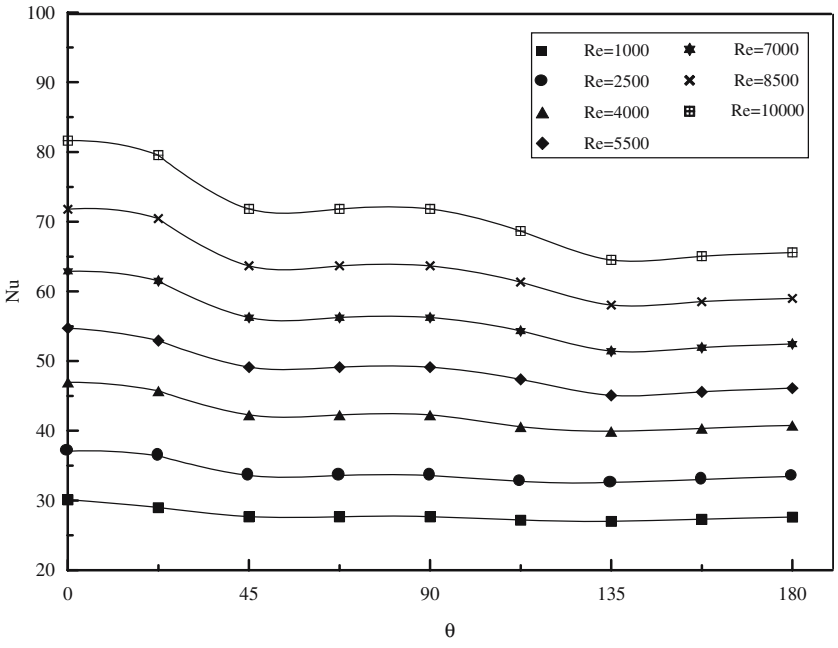

Fig. 4 Circumferential Nusselt number distribution in the case of using single slot jet aligned with cylinder axis at $W/d=0.25$ and $Z/d=4$

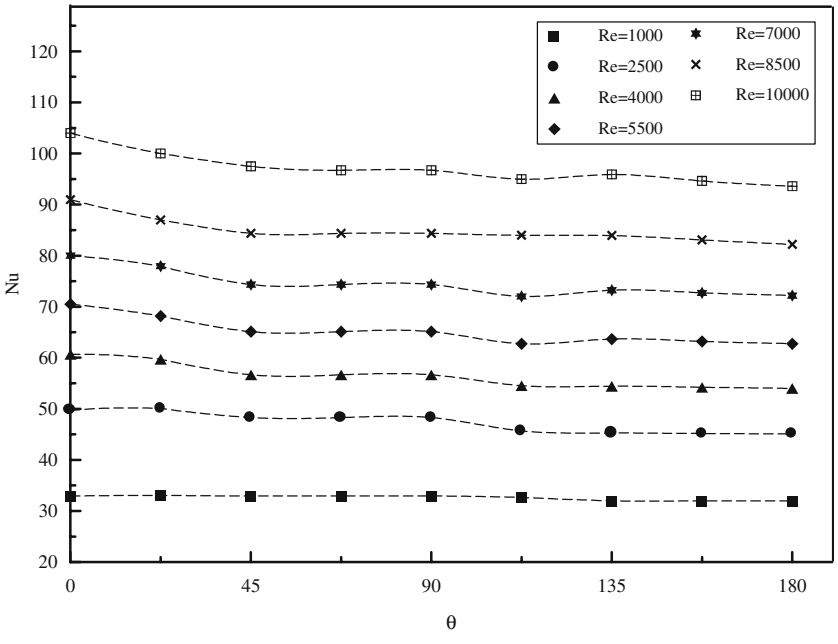

Fig. 5 Circumferential Nusselt number distribution in the case of using multiple slots jets orthogonal with cylinder axis at $W/d=0.25$ and $Z/d=4$

circumferential local Nusselt number around the cylinder decreases with decreasing Reynolds number and this indicates that there is no change of the jet flow occurs around the surface of the cylinder at low Reynolds numbers. This smooth variation of the local Nusselt reported in Fig. 4, specially at low Reynolds number, may attributed to the high thermal conductivity of the tube material which leads to circumferential heat conduction. This circumferential heat conduction becomes more significant at low Reynolds numbers. One would expect much higher circumferential variations in heat transfer coefficient than what is reported in this figure if a less conductive tube material was used. The same trend of the circumferential variation of the local Nusselt number shown in Fig. 4 was obtained for the different values of W/d and Z/W.

For configuration 2, Fig. 5 shows the circumferential variation of the local Nusselt number versus the angle θ with the Reynolds number as a parameter for $Z/W=4$ and $W/d=0.25$. As shown in the figure the Nusselt number is approximately constant around the circumference of the cylinder. The maximum and minimum Nusselt numbers were noticed at $\theta=0°$ and 180°, respectively. This trend of the circumferential local Nusselt number can be attributed to the following: (1) in the zone $0 \leq \theta \leq 90$ the flow impinge the surface of the

cylinder at each point in this cylinder surface zone with approximately the same velocity and this leads to approximately uniform Nusselt number in the zone $0 \leq \theta \leq 90$ corresponding to a stagnation Nusselt number, (2) at $\theta = 0°$ the flow has slightly higher stagnation Nusselt number because the flow at this point may have lower boundary layer thickness with slightly higher degree of turbulence than the other points of the stagnation zone, and (3) at the back of the cylinder, the Nusselt number decreased because the turbulence level is probably reduced by the vicinity of the wall. The same trend of the circumferential variation of the local Nusselt number was obtained for the different values of W/d and Z/W.

Figures 4 and 5 show that heat transfer rate gradually decreases with increasing of θ irrespectively of jet Reynolds number and jet–cylinder configurations. This monotonous variation shields the second peak, caused by the transition from laminar flow to turbulent one. This phenomenon always occurs at lower slot orifice-to-cylinder spacing and higher jet Reynolds number. Its disappearance may be attributed to the uniform distribution of the thermocouples along the circumference of the cylinder. Comparing Figs. 4 and 5, one can conclude that the circumferential distribution of the local Nusselt number in configuration 2 was more uniform than that of configuration 1. This advantage is very important in food industry where more uniform heat transfer rates leads to more uniform dehydration rate of the product. Also Figs. 4 and 5 show that the Nusselt numbers around the cylinder increased with increasing Reynolds numbers. This can be attributed to that higher Reynolds number and higher jet velocity may create a thin boundary layer, a turbulent boundary layer and higher degree of turbulence that leads to higher rates of heat transfer.

Temperature measurements at the five axial locations A–E shown in Fig. 3 reveal that there was no axial variation in the surface temperature and Nusselt number in configuration 1. The variation in the measured temperature along the axis of the cylinder was within 0.5°C. However, in the case of configuration 2 the axial Nusselt numbers were maximum at the axial locations underneath the jet (axial locations A and E), then the axial Nusselt number decreases between these two locations. At the stagnation zone $-90 \leq \theta \leq 90$ another secondary relative maximum was noticed at halfway (namely at axial location C) between the two axial locations underneath the two jets (A and E). The presence of the second maximum can be attributed to the interaction between the adjoining wall jets of each two successive slots jets, which produce more turbulence at the interaction point. Figure 6 shows the variation of the axial Nusselt numbers with the dimensional axial distance x/d between the two jets A and E (x is measured from A) at different circumferences of the cylinder for $W/d = 0.25$, $Z/W = 4$, and $Re = 10{,}000$. The trend was almost the same for other conditions with a decrease and disappearance of the second relative maximum with the decrease of Re and the increase of Z/W where the energy and momentum of the flow in the wall jet regions became too low to produce turbulence at the interaction point.

3.2 Effect of dimensionless slot orifice-to-cylinder spacing (Z/W)

The dependence of the average Nusselt number around the cylinder on the dimensionless slot orifice-to-cylinder spacing (Z/W) is shown in Figs. 7 and 8 for the three dimensionless slot widths (W/d) and the seven Reynolds number (Re) studied for the two jets–cylinder configurations, respectively. Figures 7 and 8 reveal that for all Reynolds numbers and slot widths a maximum in the mean Nusselt number occurs at a slot-to-cylinder spacing (Z) between four and six slot width (W). This variation of the Nusselt number with slot-to-cylinder spacing can be investigated based on the physics and hydrodynamics of the air jet impinging on a cylinder as shown in Fig. 9. As a free jet exits the slot from the jet plenum into a quiescent ambient, the jet is turbulent and characterized by a uniform velocity profile at the slot exit. With increasing distance from the exit, momentum exchange between the jet and the ambient causes the free boundary of the jet to broaden and the potential core, within which the uniform exit velocity is retained, to contract. The free jet or the shear layer at the boundary between the potential core and the stagnant ambient fluid is characterized by high velocity gradient and corresponding high turbulence. Downstream the potential core the velocity profile is nonuniform over the entire jet cross-section with maximum value at the center. This maximum velocity decreases with increasing distance from the slot exit. Changing the cylinder-to-slot orifice distance (Z/W), the cylinder lies at different locations within or outside the free jet potential core. Increasing Z/W in the range $0 < Z/W < H/W$, where H is the length of the potential core, the shear layer thickness increases and this increases the part of the surface area, for both jets–cylinder configurations, of the cylinder subjected to high velocity gradient and corresponding high turbulence at the shear layer. The higher turbulence increases the heat transfer rate at the front side of the cylinder ($0° < \theta < 90°$) and at the same time provides greater energy for the flow to remain attached to the cylinder as it proceeds around the cylinder surface from the forward stagnation region and this in sequence increases the rate of heat transfer from back side of the cylinder. A position near the jet exit (very small Z/W) is characterized by low-turbulence potential core flow washing the forward surface of the cylinder and the flow may deflected away from the front surface of the cylinder and can not reattach on the back side of the cylinder and this reduces the rate of heat transfer especially at low Reynolds numbers. In a position very close to the tip of the potential core ($Z/W \cong H/W$) the flow velocity is still relatively unaffected by the stagnant ambient

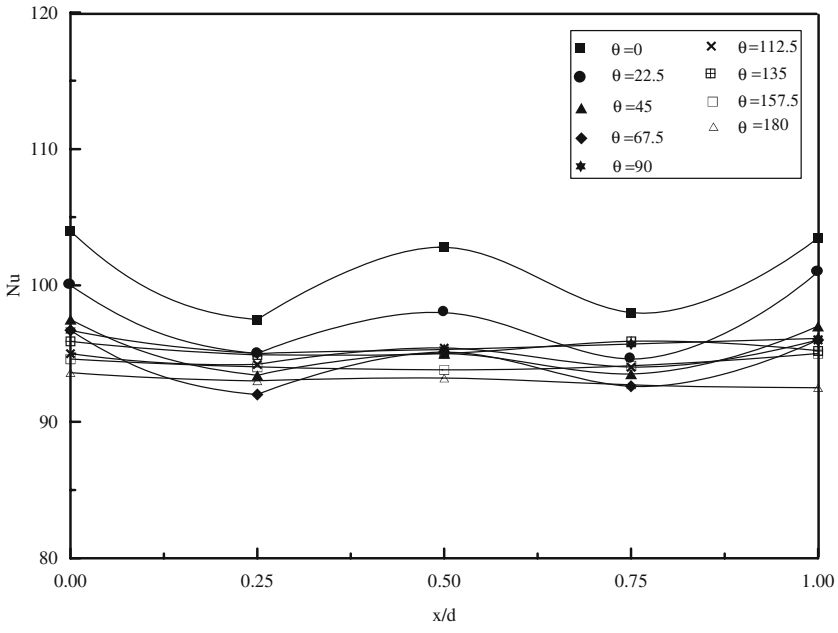

Fig. 6 Axial variation of circumferential Nusselt numbers in the case of using multiple slots jets orthogonal with cylinder axis at $W/d = 0.25$, $Z/d = 4$, and $Re = 10{,}000$

fluid, and the high turbulence generated in the shear layer at the boundary of the potential core cools much of the heated cylinder. The flow remains attached around most of the backside of the cylinder due to the high momentum and turbulence energy. This condition corresponding to the optimum heat transfer seen by the peak Nusselt number at Z/W lies in the range $4 < Z/W < 6$, observed in Figs. 7 and 8. Also Figs. 7 and 8 show that the maximum Nusselt number is more evident at higher Reynolds numbers, where the effect of the shear-induced turbulence at the tip of the potential core is more pronounced. Previous data [3, 6, 29–31] have shown that the potential core for slot jets to be approximately three to eight slot widths in length and this supports our finding of maximum Nusselt at Z/W lies in the range $4 < Z/W < 6$. Also several other authors [18, 20, 23, 25, 32] support the present results where a maximum of heat transfer rate were reported when $Z/W = 3$–8. Increasing Z/W in the range $H/W < Z/W$, the cylinder is located beyond the potential core and the jet centerline velocity degrades from its nozzle exit velocity and decreases with increasing Z/W. This may degrade the free jet momentum to a level where the high turbulence of the shear layer cannot compensate the reduction of the free jet momentum and this reduces the rate of heat transfer and the cylinder is cooled ineffectively.

3.3 Effect of cylinder curvature (W/d)

The effect of cylinder curvature (ratio of slot width to cylinder diameter; W/d) on the mean Nusselt numbers around the cylinder for different dimensionless slot-to-cylinder spacing (Z/W) and different Reynolds numbers is shown in Fig. 10 for the two jet–cylinder configurations. The diameter of the cylinder was kept constant and increasing the slot width increased the surface curvature. Figure 10 reveals that for the same dimensionless slot-to-cylinder spacing (Z/W) and at the same Reynolds number (Re), the mean Nusselt number increases with increasing the dimensionless slot width (W/d) for both jets–cylinder configurations. This can be attributed to the following: (1) for low surface curvature, the flow momentum decreases rapidly at the cylinder's forward region and the flow reaches the backside of the cylinder with very low momentum and this decreases the rate of heat transfer, (2) as the surface curvature (W/d) increases, the portion of the cylinder that may lie outside the turbulent shear layer decreases and this increases the rate of heat transfer from the cylinder, and (3) the increases of the surface curvature could augment the size of the counterrotating vortices formed at the stagnation zone (the formation of three-dimensional counterrotating vortices near the stagnation zone was previously noticed by Choi et al. [17] and Gau and Chung [18]) which increases the momentum transport in the flow structure and enhance the heat transfer process on the wall near the stagnation point. The finding of the present work of increasing the Nusselt number with the increase of surface curvature was supported by the findings of other previous works [17–19, 25, 26].

3.4 Effect of jets–cylinder configurations

The comparison of Nusselt numbers between the two jets–cylinder configurations, namely cooling the cylinder by a single slot jet aligned with axis of the cylinder (configuration 1) or by multiple slots jets aligned orthogonal to the axis of the cylinder (configuration 2), is shown in Fig. 10 for different slot widths (W/d),

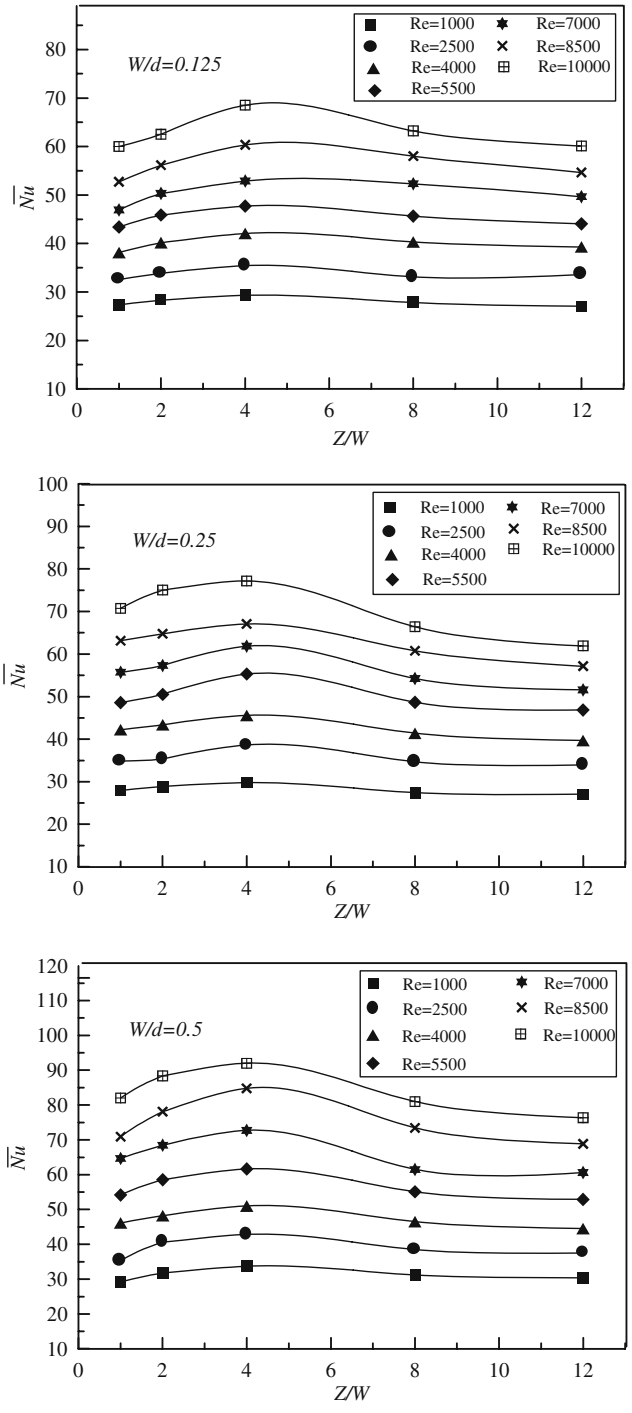

Fig. 7 Variation of average Nusselt number with Z/W for different values of W/d and Re in the case of using single slot jet aligned with cylinder axis

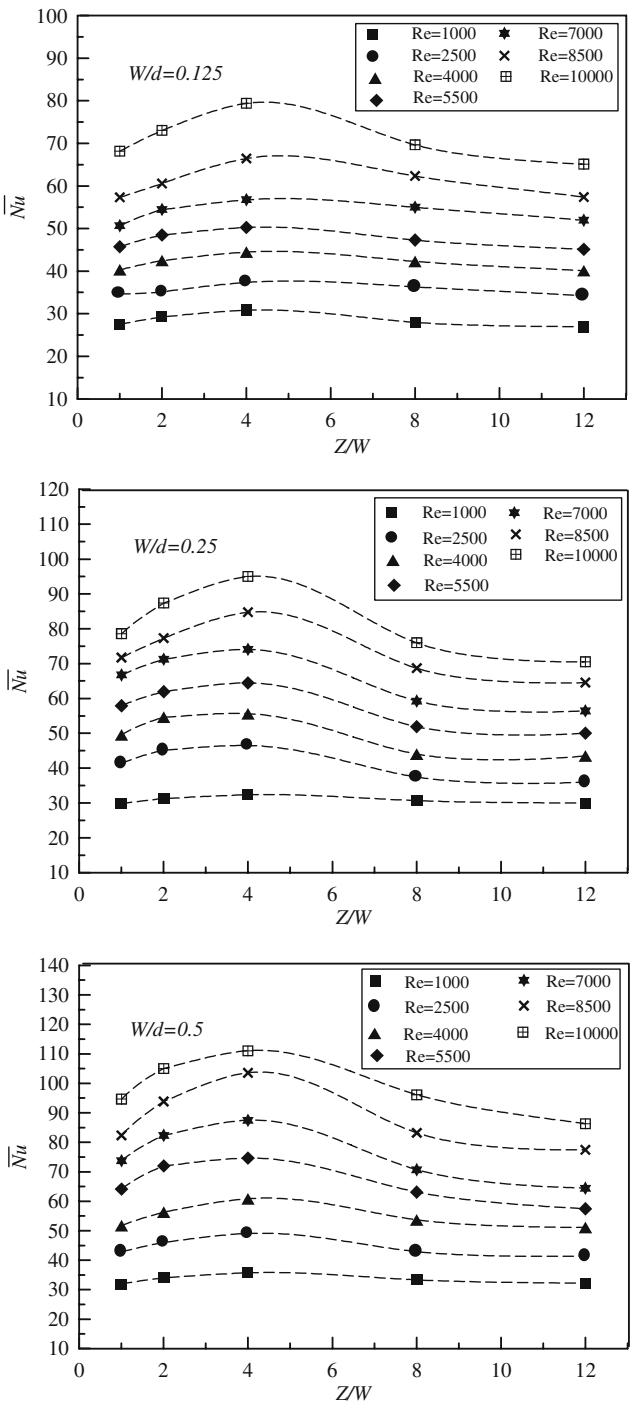

Fig. 8 Variation of average Nusselt number with Z/W for different values of W/d and Re in the case of using multiple slots jets orthogonal to cylinder axis

slot-to-cylinder spaces (Z/W) and Reynolds numbers. Figure 10 shows that at any values of Re, W/d, and Z/W the average Nusselt numbers for configuration 2 (length of each slot equals cylinder diameter and the total lengths of slots equals cylinder length) were higher than those of configuration 1 (the length of the slot equals the cylinder length). This can be attributed to the following: (1) multiple slot jets transports more flow momentum to the cylinder than single slot jet case, (2) the total length of the region of the cylinder subjected to stagnation Nusselt numbers (maximum Nusselt number) in the case of configuration 2 which equals $[n\pi d/2 = (L/d)\pi d/2 = \pi L/2]$ is higher than that of configuration 1 which equals to (L) and this leads to

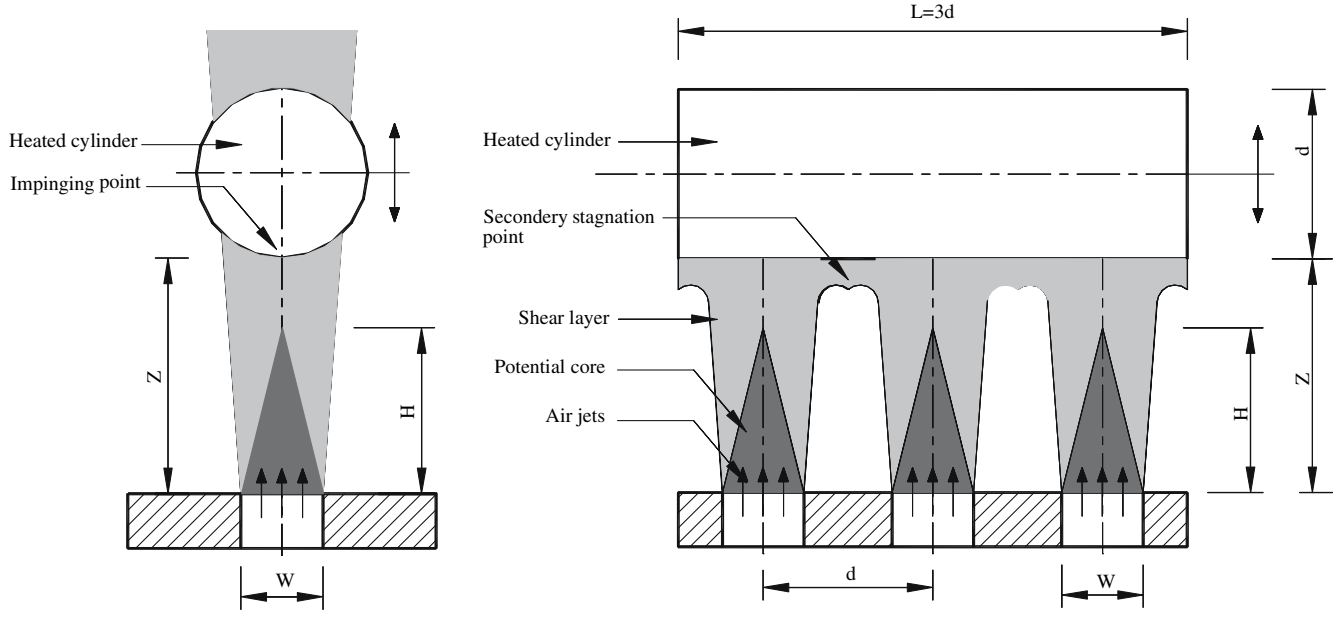

(a) Single slot jet aligned with cylinder axis (Configuration 1)

(b) Multiple slots jets orthogonal to cylinder axis (Configuration 2)

Fig. 9 Description of slot jet flow around the cylinder. **a** Single slot jet aligned with cylinder axis (configuration 1). **b** Multiple slots jets orthogonal to cylinder axis (configuration 2)

higher rate of heat transfer, (3) using multiple slot jets creates regions of secondary maximum Nusselt number zones resulting from the interaction of the adjoining wall jets of each two successive slots jets and this increases the overall mean Nusselt number, (4) the attachment of the flow to the backside of the cylinder in the case multiple slot jets orthogonal to cylinder axis is bitter than that in the case of single slot jet aligned along the axis of the cylinder as noticed from Fig. 4 where higher and bitter distribution of Nusselt number on the back side of the cylinder was noticed for multiple slots jets, and (5) The interaction of the counter-rotating vortices at the stagnation region ($0 < \theta < 90$) in the case of using multiple slots jets may create more turbulence intensity at the front side of the cylinder which leads to higher stagnation Nusselt numbers (see Figs. 4 and 5) than the case of using single slot jets.

3.5 Effect of Reynolds number

The dependence of the local and average Nusselt numbers on Reynolds number is shown in Figs. 4, 5, 7 and 8, and 10 at different values of W/d and Z/W for both jets–cylinder configurations. As shown in these figures, at the same Z/W and W/d, the Nusselt number increases with increasing Reynolds number for both jets–cylinder configurations. This can be attributed to the increase of the jet exit velocity with increasing the Reynolds number. Increasing the jet exit velocity increases both of the velocity inside the potential core and the centerline velocity downstream the potential core. Both produce higher velocity gradients in the velocity profile which leads greater shear at the shear layer and resulting higher levels of turbulence, which yield to effective cooling of the cylinder. Also increasing Reynolds number increases the momentum and the energy of the flow which make it able to attach the backside of the cylinder and leads to higher heat transfer around the cylinder. It appears from Fig. 10 that the average Nusselt number follows a $\overline{Nu} = C\,Re^m$ relationship. The empirical constant of this relationship C and m seems to be dependent on Z/W, W/d, and jets–cylinder configurations.

4 Empirical correlations

Two different empirical correlations were developed to fit the experimental data of Figs. 7, 8, and 10 for the two jets–cylinder configurations. The correlations take into account the dependence of the Nusselt number on Re, W/d, and Z/W in the ranges $1{,}000 \le Re \le 10{,}000$, $0.125 \le W/d \le 0.5$, and $1 \le Z/W \le 12$, respectively. The expressions of these correlations are as follows:

1. Single slot jet aligned with cylinder axis

$$\overline{Nu} = 1.781 Re^{0.4} \left(\frac{W}{d}\right)^{0.147} \left[1 + 0.147(Z/W) - 0.0256(Z/W)^2 + 0.0012(Z/W)^3\right]. \quad (11)$$

2. Multiple slots jets aligned orthogonal to cylinder axis

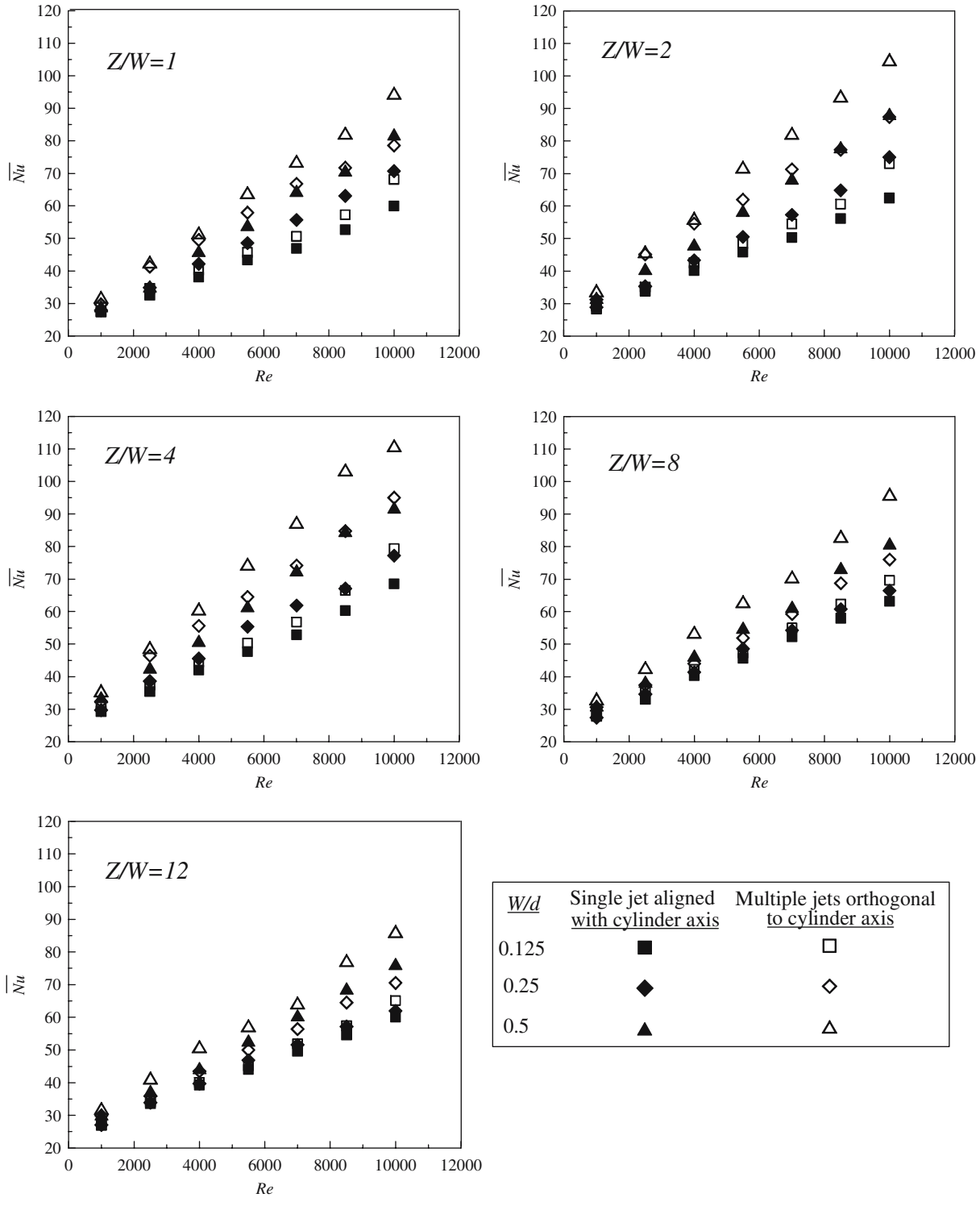

Fig. 10 Effect of surface curvature on average Nusselt number at different values of Z/W and Re for both cases of cooling arrangements

$$\overline{Nu} = 1.76\,Re^{0.42}\left(\frac{W}{d}\right)^{0.207}\left[1 + 0.197(Z/W) - 0.0346(Z/W)^2 + 0.0016(Z/W)^3\right]. \quad (12)$$

Figure 11a, b shows a comparison between the predictions of these correlations and the experimental data of the present and previous works, respectively. Figure 11a shows that the correlations can predict the

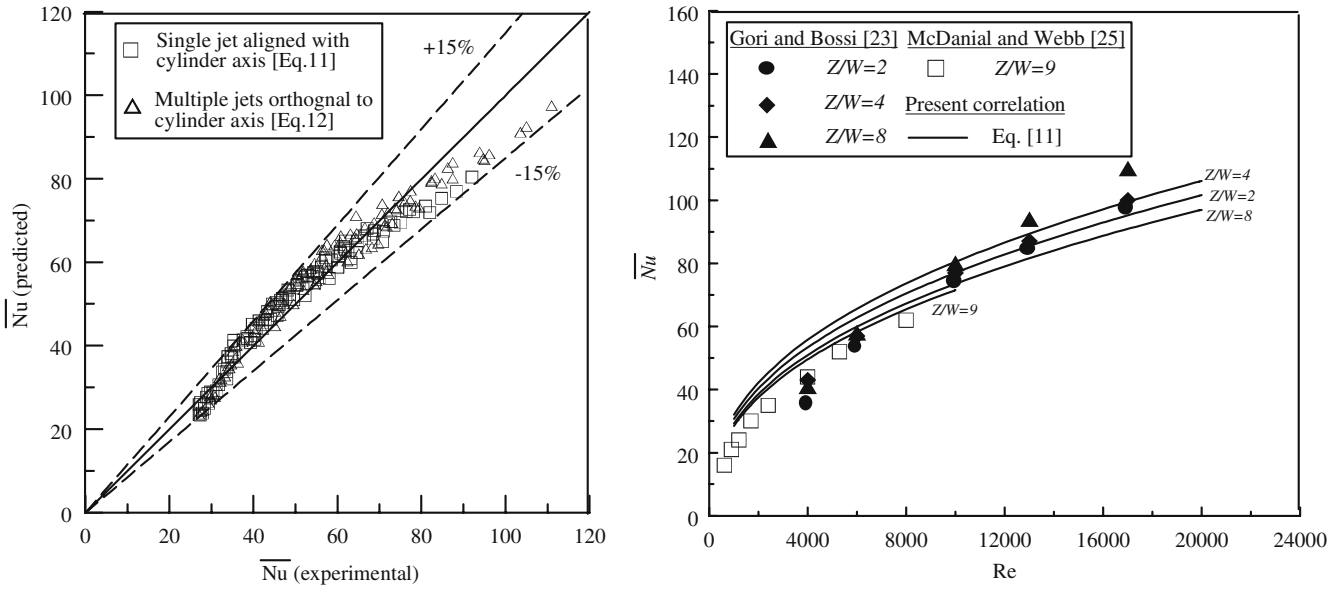

(a) Comparison with present experimental data

(b) Comparison with previous experimental data for $W/D=0.5$

Fig. 11 Comparisons between predictions of (11) and (12) with experimental data of present and previous works. **a** Comparison with present experimental data. **b** Comparison with previous experimental data for $W/D=0.5$

experimental data of the present works within ±15% for all the date of both jets–cylinder configurations. Figure 11b shows that (11) for the configuration of cooling the cylinder by a single slot jet aligned with the cylinder axis can predict both the data of Gori and Bossi [23] and McDaniel and Webb [25] for $W/D=0.5$ within ±14%. Also, although (11) correlates the data of the present work within the range $1{,}000 \leq Re \leq 10{,}000$, Fig. 11a, b shows that it predicts the data of Gori and Bossi [23] that was taken in the range $10{,}000 \leq Re \leq 20{,}000$ within ±10%.

5 Conclusions

A slot jet air impinging cooling of a cylinder has been experimentally investigated. Two different jets–cylinder configurations were studied: (1) single slot jet aligned along the axis of the cylinder, and (2) multiple slot jets aligned orthogonal to the axis of the cylinder. For comparison study, the length of the slot of the first arrangement was equal to the length of the cylinder, while in the second arrangement the length of each slot was equal to the diameter of the cylinder and the number of the slots jets was chosen to give sum of slots lengths equals the length of the single slot jet (length of the cylinder) of the first arrangement. These multiple jets were situated equally spaces along the axis of the cylinder. For each configuration, the parametric effects of Reynolds numbers (Re) ranging from 1,000 to 10,000, the dimensionless slot widths to cylinder diameter (W/d) ranging from 0.125 to 0.5, and the dimensionless slot nozzle-to-impingement cylinder spaces to the slot widths (Z/W) ranging from 1 to 12 on the local and average Nusselt numbers along the surface of the cylinder were investigated. The results showed that, for both configurations, the Nusselt number around the cylinder increased with increasing both of Re and W/d. Also the mean Nusselt number increased with increasing Z/W until it reached a maximum value at Z/W in the range $4 < Z/W < 6$ then it decreased with higher increasing of Z/W. For the first configuration, local circumferential Nusselt number decreased with increasing the angle from the impinging point. For the second configuration, the local Nusselt number was approximately constant and equal the stagnation Nusselt number around the front half of the cylinder and then the local Nusselt number decreased with increasing the angle around the backside of the cylinder. Comparisons between the two configurations showed that cooling the cylinder by multiple slots jets situated orthogonal to the axis of the cylinder gives higher and more uniform heat transfer rate around the cylinder than that of cooling the cylinder by single slot jet aligned with the axis of the cylinder when all other parameters W/d, Z/W, and Re kept the same. Correlations for the average Nusselt numbers around cylinder surface were presented for the two configurations. Comparisons between the predictions of the present correlations and the present and other previous experimental data were conducted and good agreement was found.

References

1. Chan TL, Jambunathan K, Ashforth-Frost S (1999) Jet impingement heat transfer—a bibliography: 1870–1977. Rev Heat Mass Transf 25(5):464–473
2. Chan TL, Jambunathan K, Ashforth-Frost S (1999) Jet impingement heat transfer—a bibliography: 1978–1998. Rev Heat Mass Transf 25(6):558–570
3. Downs SJ, James EH (1987) Jet impingement heat transfer—a literature survey. ASME Paper No. 87-HT-35, 10 pp
4. Jambunathan K, Lai E, Moss MA, Button BL (1992) A review of heat transfer data fir single circular jet impingement. Int J Heat Fluid Flow 13(2):106–115
5. Viskanta R (1993) Heat transfer to impinging isothermal gas and flame jets. Exp Therm Fluid Sci 6:111–134
6. Martin H (1977) Heat and mass transfer between impinging gas jets and solid surfaces. Adv Heat Transf 13:1–60
7. Metzger DE, Baltzer RT, Jenkins CW (1972) Impingement cooling performance in gas turbine airfoils including effects of leading edge sharpness. J Eng Power 94:209–225
8. Tabako W, Clevenger W (1972) Gas turbine blade heat transfer augmentation by impingement of air jets having various configurations. J Eng Power 94:51–60
9. Chupp RE, Helms HE, McFadden PW, Brown TR (1968) Evaluation of internal heat transfer coefficients for impingement cooled turbine airfoils. J Aircraft 6:203–208
10. Bunker RS, Metzger DE (1990) Local heat transfer in internally cooled turbine airfoil leading edge regions. Part I. Impingement cooling without film cooling extraction. J Turbomach 112:451–458
11. Mayle RE, Blair MF, Kopper FC (1988) Turbulent boundary layer heat transfer on curved surfaces. J Heat Transf 101:521–525
12. Metzger DE, Yamashita T, Jenkins CW (1969) Impingement cooling of concave surfaces with lines of circular air jets. J Eng Power 9:149–158
13. Hrycak P (1980) Heat transfer from a row of impinging jets to concave cylindrical surfaces. Int J Heat Mass Transf 24:407–419
14. Dyban YP, Mazur AI (1970) Heat transfer from a flat air jet flowing into a concave surface. Heat Transf Sov Res 2:15–20
15. Kayansyan N, Kucuka S (2001) Impingement cooling of a semi-cylindrical concave channel by confined slot-air jet. Exp Therm Fluid Sci 25:383–396
16. Yang G, Choi M, Lee JS (1999) An experimental study of slot jet impingement cooling on concave surface: effects of nozzle conviguration and curvature. Int J Heat Mass Transf 42:2199–2209
17. Choi M, Yoo HS, Yang G, Lee JS, Sohn DK (2000) Measurements of impinging jet flow and heat transfer on a semi-circular concave heat transfer surface. Int J Heat Mass Transf 43:1975–1985
18. Gau C, Chung CM (1991) Surface curvature effect on slot-air-jet impingement cooling flow and heat transfer process. J Heat Transf 113:858–864
19. Lee DH, Chung YS, Kim DS (1997) Turbulent flow and heat transfer measurements on a curved surface with a fully developed round impinging jet. Int J Heat Fluid Flow 18:160–169
20. Chan TL, Leung CW, Jambunathan K, Ashforth-Frost S, Zhou Y, Liu MH (2002) Heat transfer characteristics of a slot jet impinging on a semi-circular convex surface. Int J Heat Mass Transf 45:993–1006
21. Potts DW (1984) An experimental study of jet impingement on a cylinder. Report No. AFIT/CI/NR 84-50T, 192 pp
22. Sparrow EM, Altemani CAC, Chaboki A (1984) Jet-impingement heat transfer for a circular jet impinging in cross flow on a cylinder. J Heat Transf 106:570–577
23. Gori F, Bossi L (2000) On the cooling effect of an air jet along the surface of the cylinder. Int Commun Heat Mass Transf 27:667–676
24. Sparrow EM, Alhomoud A (1984) Impingiment heat transfer at a circular cylinder due to an offset or non-offset slot jet. Int J Heat Mass Transf 27:2297–2306
25. McDaniel CS, Webb BW (2000) Slot jet impingement heat transfer from circular cylinder. Int J Heat Mass Transf 43:1975–1985
26. Olsson EEM, Ahrne AM, Tragardh AC (2004) Heat transfer from a slot air jet impinging on a circular cylinder. J Food Eng 63:393–401
27. Olsson EEM, Ahrne LM, Tragardh AC (2005) Flow and heat transfer from multiple slot air jets impinging on circular cylinder. J Food Eng 67:273–280
28. Holman JP, Gajda WC (1989) Experimental method for engineering. McGraw Hill, New York
29. Livingood JNP, Hrycak P (1973) Impingement heat transfer from turbulent air jets to flat plates—a literature suvey, NASA TM x-2778
30. Baughn J, Shimizu S (1989) Heat transfer measurements from a surface with uniform heat flux and an impinging jet. ASME J Heat Transf 111:1096–1098
31. Yan X, Baughn JW, Mesbah M (1992) The effect of Reynolds number on the heat transfer distribution from a flat plate to an impinging jet. ASME Pap HTD 226:1–7
32. Lee DH, Chung YS, Kim MG (1999) Turbulent heat transfer from a convex hemispherical surface to a round impinging jet. Int J Heat Mass Transf 42:1147–1156